Tribology Online

Japanese Society of Tribologists
http://www.tribology.jp/trol/

Vol. 15, No. 5 (2020) 380-387.
ISSN 1881-2198
DOI 10.2474/trol.15.380

Article

Dynamic Performance of an Externally Pressurized Porous Thrust Bearing Employing Different Pocket Shape

Vivek Kumar[1)*], Vatsalkumar Ashokkumar Shah[2)], Kuldeep Narwat[3)] and Satish C. Sharma[4)]

[1)] Assistant Professor, Department of Mechanical Engineering, School of Technology,
Pandit Deendayal Petroleum University, Knowledge Corridor, Raisan Village, Gandhinagar 382007 Gujarat (State), India
[2)] M. Tech (Scholar), Department of Mechanical Engineering, School of Technology,
Pandit Deendayal Petroleum University, Knowledge Corridor, Raisan Village, Gandhinagar 382007 Gujarat (State), India
[3)] Assistant Professor, School of Mechanical Engineering, Galgotias University, Plot No. 2, Yamuna Expressway, Opposite,
Buddha International Circuit, Sector 17A, Greater Noida, Uttar Pradesh (State) 203201, India
[4)] Professor, Mechanical and Industrial Engineering Department, Indian Institute of Technology (IIT) Roorkee,
Roorkee - Haridwar Highway, Roorkee, Uttarakhand 247667 India

*Corresponding author: Vivek Kumar (vivek.kumar@sot.pdpu.ac.in)

Manuscript received 14 July 2020; accepted 21 October 2020; published 30 November 2020

Abstract

The use of porous facing/layer in fluid film bearings offers some unique advantages such as self-lubricating properties (acting as lubricant reservoir), compactness, economical over conventional bearing etc. This article presents a numerical simulation of an externally pressurized porous thrust bearing. The collective effect of permeability of porous facing and lubricant supplying pocket shape has been investigated on steady-state and dynamic performance indices of bearing. Flow governing equation i.e. Reynolds equation, Darcy's Law and fluid flow equation (through an orifice device) has been solved simultaneously (using finite element approach) to compute fluid film pressure distribution. The bearing performance indices i.e. film reaction force, lubricant flow, stiffness and damping parameters are computed as a function of permeability and geometric shape of pocket. It has been reported that high value of permeability of porous facing have an adverse effect on the load supporting capacity, lubricant flow, stiffness and damping parameters of the bearing. There exist a range of permeability value ($(2.2\sim3)10^{-14}$ m^2; $\psi = 0.001\sim0.01$) within which the adverse effect of using porous facing can be partially reduced/mitigated by appropriate selection of pocket shape (Circular and square) in thrust pad.

Keywords

porous thrust bearing, permeability, pocket geometry, FEM

1 Introduction

Externally pressurized thrust bearings rely on continuous supply of pressurized lubricant from pump, to support external loads in machines such as turbo-generators, vertical pumps, hydraulic rotors etc. They are also used to produce hydrostatic oil lift while precisely controlling the movement or orientation of structures such as telescopes, observatory domes, antenna etc. The high load supporting capacity per unit area, zero friction and wear (during start up and shut down operation of machines), good dynamic characteristics [1] are some of the unique advantages associated with hydrostatic bearing systems vis-à-vis hydrodynamic bearing systems. The design of hydrostatic/hybrid thrust bearings have continuously evolved ever since their first use. Some initial research carried by Rowe [1] were substantially helpful in standardizing the design and application practices of hydrostatic/hybrid bearings. These research activities [1] form the foundation/basis of further significant research carried by many researchers [2-5], in the design of such bearings. In order to achieve desired performance level from hydrostatic thrust bearings, an adequate selection of flow control device, pump capacity, lubricating oil and pocket geometry is of utmost importance. A flow control device is required to effectively control the performance of such system under dynamic operation of bearings. Many investigations were reported examining the effect of flow control devices namely capillary tube [2], flow control valve [3], membrane [4], orifice plate [5], etc., on the operational performance of these bearings. It has been reported that the stiffness characteristics of bearing strongly depends upon the type of flow control device employed in the bearing system. Recently, Kumar and Sharma [5] carried out a numerical investigation on capillary and orifice controlled hydrostatic lubrication of thrust bearing under the influence of magnetic field.

The pressurized lubricant in hydrostatic bearing are generally regulated via flow control device to the pocket of the bearings. Conventionally, pockets in thrust pads are made rectangular in shape because of ease in the manufacturing. Nowadays, sophisticated manufacturing techniques are available, which have the capabilities to produce non-conventional pockets at the will/convenience of the bearing designers or practicing engineers. Manufacturing techniques such as microstereolithography [6], micro-machining [7], Laser surface texturing [7, 8] can produce macro as well as micro-features on the surface of pad with very tight tolerances or dimensional accuracy. The availability of such manufacturing techniques [6-8] have enabled bearing design to copy even bionic feature over the bearing surface. Since last two decades, theoretical and experimental efforts are made to reduce coefficient of friction and enhance load supporting ability of bearings, by producing micro-features/patterns [9, 10] on bearing surface. With these modern manufacturing techniques, many investigations were reported exploring the use of non-conventional pocket shapes such as circular, annular, multi-pocket [2, 11, 12] etc. in pads of hydrostatic bearing. These studies reported that use of these non-conventional pocket shapes provide better dynamic characteristics to a hydrostatic bearing.

The porous facing/layer is widely used in thrust and journal bearings employed in engineering applications such electric motors in household appliances, medical instruments, machine tools, textile and food industry etc. The porous matrix in such bearing facings acts as sponge and possess tendency to store the lubricating oil. This is quite useful for bearings operating under sealed or starved lubrication conditions. Apart from this, porous bearings are economical and occupy less space vis-à-vis to conventional bearings. The flow of lubricant in porous medium is generally expressed using Darcy model [13, 14] and Brinkman model [15]. The Darcy model use no-slip condition at porous layer and lubricating film interface, whereas Brinkman model takes into account viscous shear term across the porous-matrix. Many investigations have been reported applying porous layer on the performance of slider bearings [14], Journal bearing [13, 16], step-slider bearing [17], squeeze film operation of parallel plates [18, 19], exponential slider bearings [20], etc. These studies have investigated the effect of permeability of porous layer on the load supporting capacity and friction coefficient. It has been reported that an increase in permeability of porous matrix leads to a reduction in load supporting capacity and enhancement in the friction coefficient [13, 15-17, 20]. It is also reported that use of porous facing leads to a reduction in the squeeze film response time of parallel plates [18, 19]. Hanawa et al., [21] performed theoretical and experimental simulations of porous surface rectangular hydrostatic thrust bearing operated with capillary tube as a compensating element. The authors have compared the performance of impermeable pocket thrust bearing with conventional porous thrust bearing and newly conceived thrust bearing with porous land region. The authors have concluded that the proposed porous land thrust bearing structure offers comparable load carrying capacity and stiffness characteristics (as of conventional porous thrust bearing) while operating with a clearance of less than 15 μm.

The literature review discussed above reported that substantial research activities were carried out exploring use of porous facings in hydrodynamic thrust bearings/ squeeze film bearings [14, 17-20]. In spite of reducing the load supporting capacity and enhancing friction coefficient, they are widely used because of their self-lubricating characteristics and economical aspect as compared to conventional bearings. To the best of author knowledge, very few studies are available examining the effect of porosity on dynamic performance indices of a compensated hydrostatic thrust bearings. This study is aimed to compute effect of permeability of the porous facing on the rotor-dynamic (stiffness and damping) parameters of an externally pressurized thrust pad employing different pocket geometry.

2 Analysis

Figure 1(a) presents schematic representation of a porous thrust bearing under consideration. Different pocket shape

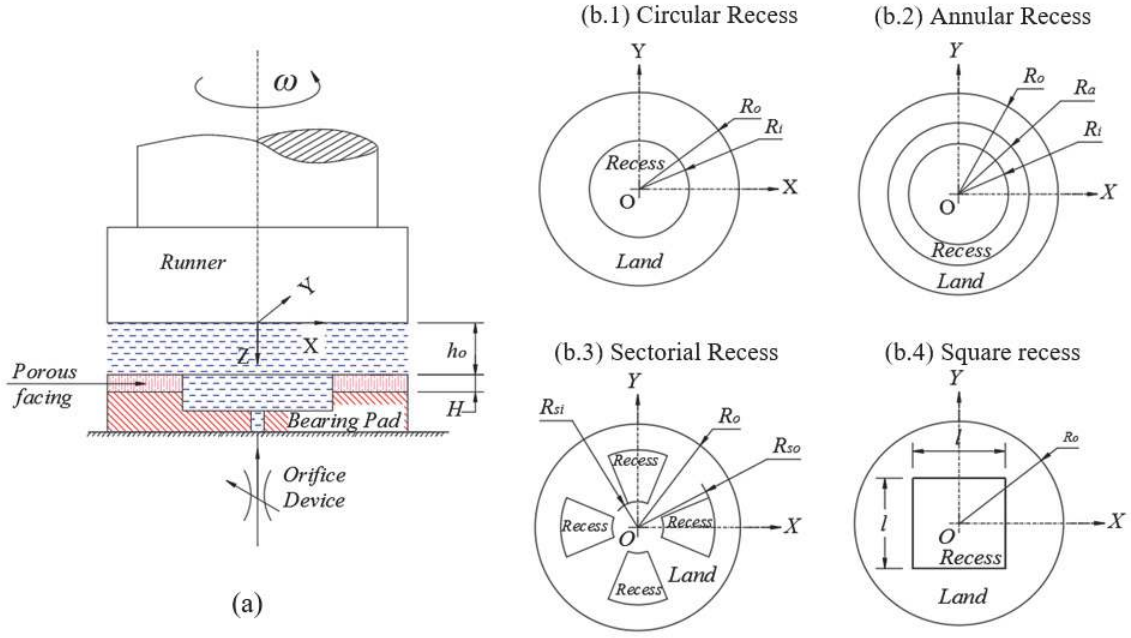

Fig. 1 (a) Bearing schematic (b) Recess configuration

(Circular, Annular, Sectorail and Square) under investigations are shown in Fig. 1(b). The lubricant is supplied to pocket/land area via an orifice device, which is employed as flow control device. A porous layer having thickness (H) and permability (k) has been provided on the land area of pad. The lubricant flow is considered to be laminar, incompressible and isothermal through the clearnace space as well as in the porous matrix.The genearlized Reynolds equation for hydrostatic thrust bearing (with no-slip assumption) can be expressed as [22]:

$$\frac{\partial}{\partial x}\left(\frac{h^3}{12\mu}\frac{\partial p}{\partial x}\right)+\frac{\partial}{\partial y}\left(\frac{h^3}{12\mu}\frac{\partial p}{\partial y}\right)=W_r-W_t \tag{1}$$

Where W_r and W_t are the squeeze velocity at runner and thrust bearing. The squeeze velocity at runner surface can be defined as: $\partial h/\partial t$, where as the squeeze velocity at thrust surface is governed by Darcy's Law and continuity equation. The velocity at fluid at porous facing is given by [14]:

$$u_n=-\frac{k}{\mu}\frac{\partial P}{\partial n}=W_t \tag{2}$$

Where n referes indices for x, y and z direction. P is fluid pressure in porous facing matrix.

Continuity equation:

$$\nabla.\, u=\frac{\partial}{\partial x}\left(-\frac{k}{\mu}\frac{\partial P}{\partial x}\right)+\frac{\partial}{\partial y}\left(-\frac{k}{\mu}\frac{\partial P}{\partial y}\right)+\frac{\partial}{\partial z}\left(-\frac{k}{\mu}\frac{\partial P}{\partial z}\right)=0 \tag{3}$$

Integrating above equation along the porus layer thickness yields,

$$\frac{k}{\mu}\frac{\partial P}{\partial z}=-H\left[\frac{\partial}{\partial x}\left(-\frac{k}{\mu}\frac{\partial P}{\partial x}\right)+\frac{\partial}{\partial y}\left(-\frac{k}{\mu}\frac{\partial P}{\partial y}\right)\right] \tag{4}$$

Combining Eqs. (1) and (3) yields

$$\frac{\partial}{\partial x}\left(\left\{\frac{h^3}{12\mu}+\frac{kH}{\mu}\right\}\frac{\partial p}{\partial x}\right)+\frac{\partial}{\partial y}\left(\left\{\frac{h^3}{12\mu}+\frac{kH}{\mu}\right\}\frac{\partial p}{\partial x}\right)=\frac{\partial h}{\partial t} \tag{5}$$

In non-dimensional form the above equation can be represented as:

$$\frac{\partial}{\partial \bar{x}}\left(\{\bar{h}^3+\psi\}\frac{\partial \bar{p}}{\partial \bar{x}}\right)+\frac{\partial}{\partial \bar{y}}\left(\{\bar{h}^3+\psi\}\frac{\partial \bar{p}}{\partial \bar{y}}\right)=\frac{\partial \bar{h}}{\partial \bar{t}} \tag{6}$$

Where: $\bar{x}=\frac{x}{R_o};\ \bar{y}=\frac{y}{R_o};\ \bar{h}=\frac{h}{h_r};\ \bar{p}=\frac{p}{p_s};\ \psi=\frac{kH}{\mu h_r^3};\ \bar{t}=t\,\frac{h_o^2 p_s}{\mu r_o^2}$

Equation (6) is subjected to finite element formulation to reduce it in form of set of algebric equations. The pad surface is divided into small/finite regions using four noded quad elements of isoparametric nature. The film pressure within each element is approximated as follows:

$$\bar{p}=\sum_{i=1}^{4}[N_i\bar{p}_i];\ \mathrm{N_j}=\frac{1}{4}(1+\xi_i\xi)(1+\eta_i\eta) \tag{7}$$

Galerkin apprach of Weighted residual method is applied to obtain weak form of Eq. (6).

$$\iint N_i\left(\frac{\partial}{\partial \bar{x}}\left(\{\bar{h}^3+\psi\}\frac{\partial}{\partial \bar{x}}\left\{\sum_{i=1}^{4}(\bar{p}_iN_i)\right\}\right)+\frac{\partial}{\partial \bar{y}}\left(\{\bar{h}^3+\psi\}\frac{\partial}{\partial \bar{y}}\left\{\sum_{i=1}^{4}(\bar{p}_iN_i)\right\}\right)-\frac{\partial \bar{h}}{\partial \bar{t}}\right)d\bar{x}d\bar{y}=0 \tag{8}$$

Above equation can be simplified as follows:

$$[\bar{F}_{ij}^{e}]\{\bar{p}\}=[\bar{Q}_i^{e}]+\dot{\bar{h}}\,[\overline{RS}_i^{e}] \tag{9}$$

In order to accurately simulate a hydrostatic bearing, the Eq. (9) should to be coupled with fluid flow through an orifice device. This is done because the lubricant is supplied to hydrostatic bearing through the flow control devices. A flow control device is required to effectively control the stiffness and damping performance of lubricant under dynamic state. The coupling of an orifice device with bearing system ensures, lubricant flow continuity through the bearing and orifice device. This is done by locating all the nodes on the periphery/edge of pocket and collectively assgning them lubricant flow rate through the orifice device. The fluid flow rate through an orifice is govened by following expression [1, 2]:

$$\bar{Q}_R=C_d\,(1-\bar{p}_{oj})^{1/2} \tag{10}$$

Equation (9) after assembly can be expended as follows:

$$\begin{bmatrix}\bar{F}_{11}&\bar{F}_{12}&\cdots&\bar{F}_{1j}&\cdots&\bar{F}_{1n}\\ \bar{F}_{21}&\bar{F}_{22}&\cdots&\bar{F}_{2j}&\cdots&\bar{F}_{2n}\\ \vdots&\vdots&\vdots&\vdots&\vdots&\vdots\\ \bar{F}_{j1}&\bar{F}_{j2}&\cdots&\bar{F}_{jj}&\cdots&\bar{F}_{jn}\\ \vdots&\vdots&\vdots&\vdots&\vdots&\vdots\\ \bar{F}_{n1}&\bar{F}_{n2}&\cdots&\bar{F}_{nj}&\cdots&\bar{F}_{nn}\end{bmatrix}\begin{bmatrix}\bar{p}_{o1}\\ \bar{p}_{o2}\\ \vdots\\ \bar{p}_{oj}\\ \vdots\\ \bar{p}_{on}\end{bmatrix}=\begin{bmatrix}\bar{Q}_1\\ \bar{Q}_2\\ \vdots\\ \bar{Q}_R\\ \vdots\\ \bar{Q}_n\end{bmatrix}+\dot{\bar{h}}\begin{bmatrix}\overline{RS}_1\\ \overline{RS}_2\\ \vdots\\ \overline{RS}_j\\ \vdots\\ \overline{RS}_n\end{bmatrix} \tag{11}$$

The Reynolds boundary condition (RBC) has been applied on the outer boundary of thrust pad. This ensure film pressure to approach smoothly to the ambient pressure. The steady-state performance parameters such as film pressure distribution and reaction force has been computed while disregarding runner normal/squezze velocity (last term) from Eq. (11). Thereafter, Newtons-Raphson iterative technique is used to compute film pressure distribution in bearing system.

$$\textbf{Film Reaction}:\ \bar{F}_0=\sum_{e=1}^{4}\left\{\int_{-1}^{+1}\int_{-1}^{+1}\left(\sum_{i=1}^{4}\bar{p}_iN_i\right)|\bar{J}|\,d\xi\,d\eta\right\}+\sum_{e=1}^{n_r}\bar{A}_p\bar{p}_r \tag{12}$$

Perturbation technique has been employed to numerically evaluate pressure gradient with respect to film thickness and runner squeeze/normal velocity. These computed film pressure gardient has been used to evaluate stiffness and damping parameters of the fluid film, described as follows:

$$\textbf{Stiffness Coefficient}:\ \bar{K}=\sum_{e=1}^{4}\left\{\int_{-1}^{+1}\int_{-1}^{+1}\left(\sum_{i=1}^{4}\frac{\partial \bar{p}_j}{\partial \bar{h}}N_i\right)|\bar{J}|\,d\xi\,d\eta\right\}+\sum_{e=1}^{n_r}\bar{A}_p\frac{\partial \bar{p}_r}{\partial \bar{h}} \tag{13}$$

$$\textbf{Damping Coefficient}:\ \bar{D}=\sum_{e=1}^{4}\left\{\int_{-1}^{+1}\int_{-1}^{+1}\left(\sum_{i=1}^{4}\frac{\partial \bar{p}_j}{\partial \bar{h}}N_i\right)|\bar{J}|\,d\xi\,d\eta\right\}+\sum_{e=1}^{n_r}\bar{A}_p\frac{\partial \bar{p}_r}{\partial \bar{h}} \tag{14}$$

Gauss-Legrende quadrature has been used to compute integarls in abovementioned equations.

3 Solution methodology

The solution scheme adopted to perform numerical simulation of porous hydrostatic thrust bearing is shown in Fig. 2. An iterative program based on finite element has been developed to numerically simulate the bearing system. The dimensional details of various pocket shape and bearing operating parameters are listed in Table 1. All pockets shapes have identical pocket and land areas. The land area of pad has been discretized using two dimensional (4 node) quad elements. The values of porous layer thickness (H), ranging from 0.4 mm to 2 mm corresponds to range of non-dimensional

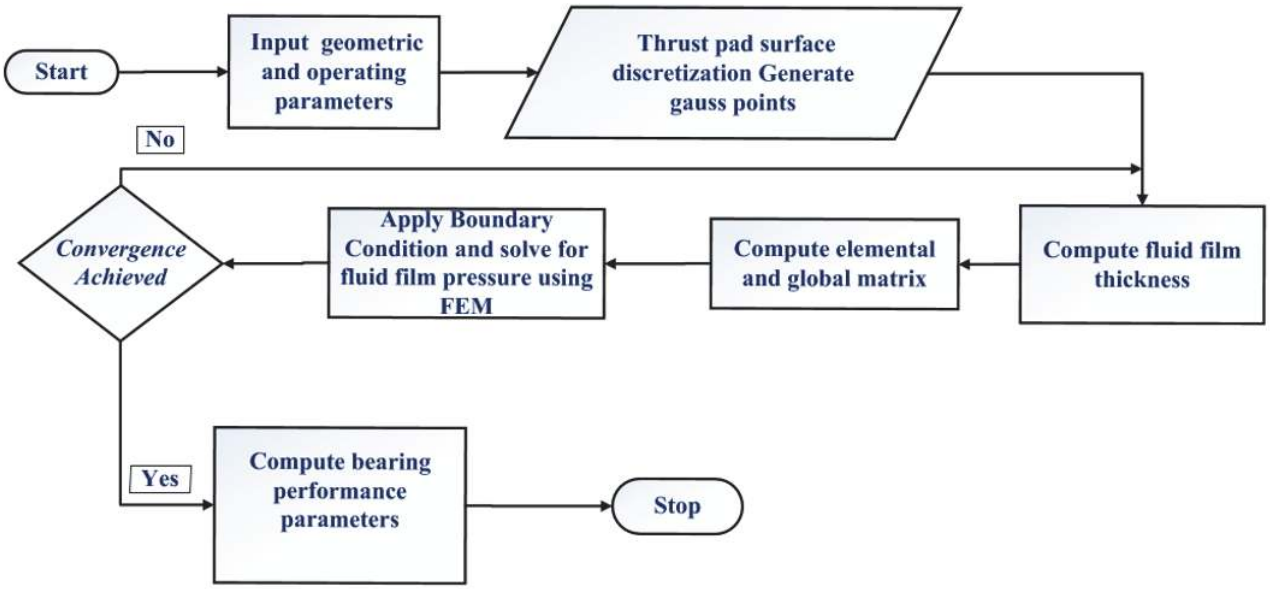

Fig. 2 Computational scheme

Table 1 Reference values of bearing geometric and operating conditions

Input parameters	Dimensional value
Radius of pad (R_o)	100 mm
Circular pocket radius (R_i)	50 mm
Sectorial pocket details	R_{so} = 75 mm; R_{si} = 25 mm
Annular pocket details	R_{so} = 71 mm; R_{si} = 50 mm
Square pocket details	l= 88.6 mm
Film thickness	0.05 mm
Supply pressure	1 MPa
Lubricant viscosity	0.034 Pa.s
Permeability (k)	(20-340)*10^{-16}m^2
Porous layer thickness	0.4 ~ 2 mm

permeability parameter (ψ), ranging from 0.0001 to 0.01. The optimum number of nodes/element are selected for each pocket after carrying out mesh-sensitivity test. The global system of equations is solved using Newton-Raphson method for the film pressure distribution. A convergence of 10^{-06} has been set on film pressure values between successive iterations, to ensure repeatability of numerical results from the iterative scheme.

A comprehensive literature has been reviewed to select a suitable paper for validating the source code. The developed source code is used to regenerate the published result from theoretical and experimental investigation carried on hydrostatic thrust bearing by Daering and Zhenming [3]. The authors have computed film pressure and lubricant flow characteristics for above-said bearing, operating with non-Newtonian lubricant. The lubricant has been formulated by adding graphite powder in ethylene glycol. Mathematically, the non-Newtonian lubricant has been described by using power law fluidic model. Source code is used to perform numerical simulation of hydrostatic thrust bearing using geometric & operating conditions of the reference bearing system [3]. Figure 3(a) indicates that lubricant supply pressure vs flow rate curves from two studies are closely following each other. A minor deviation has been reported owing to use of different numerical scheme and settling phenomenon of graphite powder in ethylene glycol. The validity of proposed model for simulating a porous surface hydrostatic thrust bearing has been checked by reproducing the numerical results from another reference study [21]. Hanawa et al. [21] had performed an experimental and numerical investigation to simulate the performance of rectangular shape hydrostatic thrust bearing. The porous layer has been applied over the land region of the pad. The lubricant has been supplied into the rectangular pocket using capillary tube as a restrictor. The developed source code has been used to

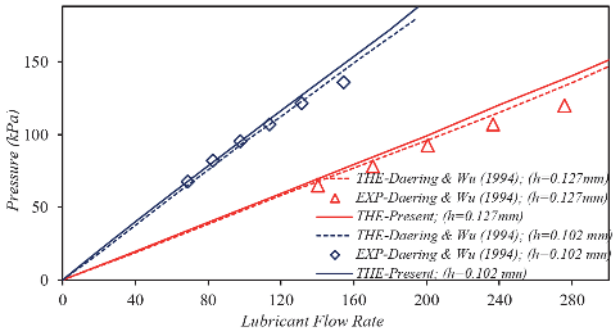

Fig. 3(a) Pump pressure vs. lubricant (graphite/ethylene glycol mixture) flow rate

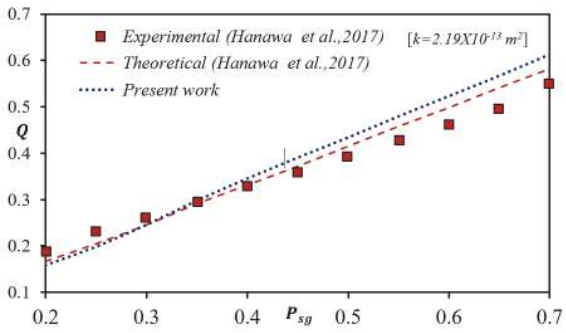

Fig. 3(b) Relationship between supply pressure (MPa) and volume flow rate (ltr/min)

generate the numerical results for supply pressure vs lubricant flow rate through the reference bearing system. A comparison of numerical and experimental results from developed source code and reference study [21] (depicted in Fig. 3(b)) shows good concordance. A maximum deviation of -5.5% has been reported between the numerical results from the two studies. The deviation can be accounted for different solution approach (FEM vs FDM) and mesh size used in two studies. The comparison of results depicted in Fig. 3(a) & (b) indicates that developed source can numerically simulate the behaviour porous hydrostatic thrust bearing with reasonably good accuracy.

4 Results and discussions

This section discusses the numerical results for hydrostatic thrust bearing under combine influence of permeability of porous facing/layer and geometric shape of pocket. The performance of various pockets in thrust pads have been compared w.r.t performance parameters such film pressure ($\overline{p}$), reaction force ($\overline{F}_o$), stiffness ($\overline{K}$) and damping ($\overline{D}$) parameters etc. The non-dimensional permeability parameter (ψ) has been varied from a value of zero to one. The bearing with solid/impermeable pad is simulated by assigning a value of zero to permeability parameter. Performance comparison have been made between different pocket shape in thrust pad while operating under identical operating conditions.

Figure 4 illustrates the effect of permeability of porous facing (ψ) and pocket geometry on three dimensional film pressure distribution on pocket and land area. It can be clearly seen that use of porous facing leads to a reduction in the pressure values and gradient over the pocket and land area. This effect is noticed to be common to all pocket geometry but with varying magnitude. It has been observed that maximum and minimum pressure has been observed for Circular and Annular pocketed thrust pad respectively. However, the maximum reduction (-3.51%) in pocket pressure is noticed for sectorial pocket thrust pad. This implies that reduction in pressure values due to use of porous facing also depends upon the geometric shape of pocket. The reduction in pressure values occurs because of slippage of lubricant into porous matrix pores, which offer lesser fluidic resistance to flow as compared to the solid/impermeable thrust pad surfaces.

Figure 5 presents numerical results for fluid film reaction force as a function of pocket shape and permeability parameter. The film reaction force is a measure of load supporting ability of bearing at a constant film thickness. It is noticed that use of porous facing has insignificant influence on fluid film reaction at lower value ($\psi < 0.01$) of permeability parameter. This implies that at such values of permeability the porous facing offers almost same resistance to fluid flow as that offered by the solid surface. However, at higher values ($\psi > 0.05$) of permeability parameter, a sharp reduction in film reaction force has been observed. It can be due to reduction in the values of film pressures over the land and pocket areas of pad. It has been noticed that circular and sectorial pocket thrust offers maximum and minimum reaction force respectively. The drop in reaction force due to use of porous facing ($\psi < 0.1$) is noticed to be lying in-between -3.8% (circular) and -4.2% (Sectorial). Effect of film thickness on fluid film reaction has been presented in Table 2. It can be clearly seen that a reduction in fluid film thickness leads to higher fluid film pressure generation which ultimately enhances the fluid film reaction values.

The numerical results for lubricant flow rate through the bearing has been depicted in Fig. 6. It can be clearly seen that for higher values of ($\psi > 0.05$) a substantial rise in fluid flow rate has been noticed. This can be attributed to slippage/leakage of lubricant through pores of porous layer, as it offers lesser resistance to fluid flow as compared to impermeable/solid surfaces. This would lead to higher pumping requirements/pumping losses by the bearing system. However, this increment in lubricant flow rate can be partially compensated by judicious selection of pocket geometry. For instance, increase in lubricant flow rate due to porous facing is minimum (+2.1%) and maximum (+4.1%) for sectorial and circular pocket thrust pads. Therefore, from perspective of lubricant flow rate, sectorial pocket can be better choice in porous bearing system. Table 2 presents numerical result for lubricant flow rate different pocket as a function of film thickness. An increase in film thickness is shown to be increasing the lubricant flow rate for various pocket shape. This can be attributed to an increase in film pressure differential between pocket and outer boundary (ambient pressure) because of an increase in film thickness value.

Figure 7 depicts numerical trends for stiffness parameter of porous hydrostatic bearing employing various pocket shapes. The numerical values of stiffness parameter depend upon gradient of reaction force with respect to film thickness. The stiffness parameters have been computing by perturbing the film thickness. The trends of stiffness parameter are in line with trends of reaction force as depicted in Fig. 5. Again, a sharp drop in stiffness capability is reported because of use of porous facing with higher permeability ($\psi > 0.05$). This effect is observed to be greater in circular and square pocket vis-à-vis annular and sectorial pocket shape in pad. Among various pocket, circular and square shapes are reported to be providing higher values of stiffness parameter. Furthermore, effect of film thickness on stiffness coefficient has been depicted in Table 2. The numerical results suggest an optimum value of film thickness at which maximum stiffness coefficient can be generated from the bearing system. This optimum value of stiffness coefficient can be clearly seen to be function of geometric configuration of pockets.

Figure 8 presents influence of porosity and geometric shape of pocket on damping parameter on the bearing system. The effect of porosity/permeability is noticed to be more adverse on damping parameter for annular and sectorial pockets vis-à-vis circular and square pockets in thrust pad. Despite this, circular and square pockets provide substantially higher damping capabilities as compared to annular pocket pad. Therefore, square pockets should be opted while designing porous thrust bearing, from the viewpoint of achieving better/higher film damping capabilities. The effect of film thickness on damping capabilities is presented in Table 2. It can be seen that damping coefficient enhance significantly owing to reduction in film thickness value. The enhancement in damping coefficient is noticed to be maximum for circular pocket shape and minimum for sectorial pocket thrust pad.

5 Conclusions

The numerical results from the present work can be consolidated as follows:

- The use of porous facing/layer with high permeability can adversely affect the load supporting capacity, lubricant flow and dynamic parameters/coefficient of an externally pressurized thrust bearing.

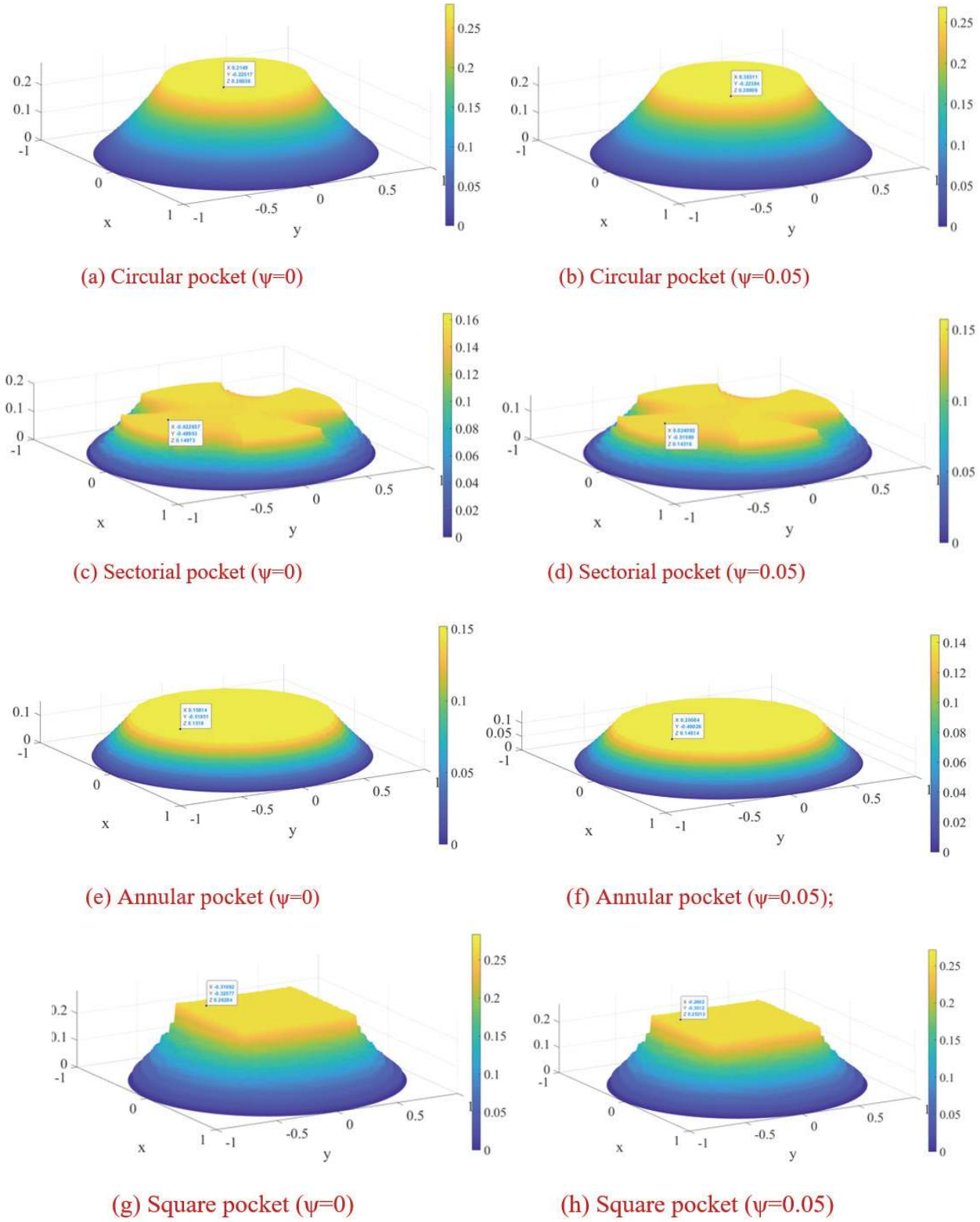

Fig. 4 Pressure profile of porous and impermeable thrust pad for different pocket geometry

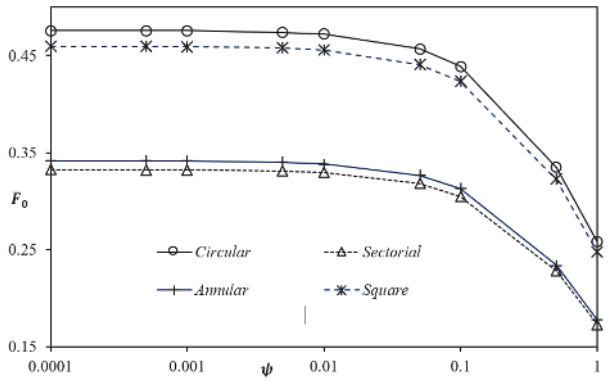

Fig. 5 Film reaction force vs permeability parameter

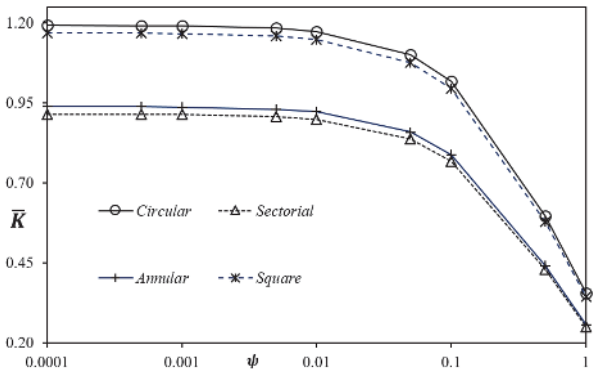

Fig. 7 Stiffness parameter vs permeability parameter

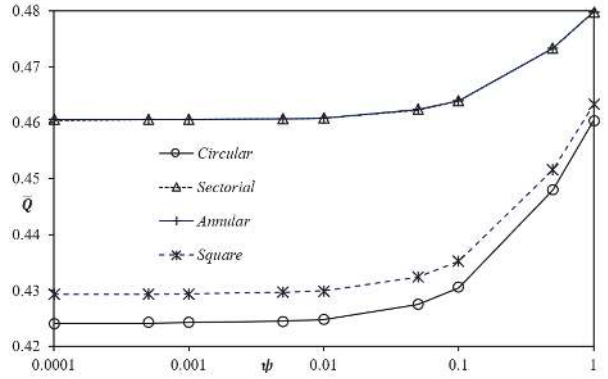

Fig. 6 Lubricant flow vs permeability parameter

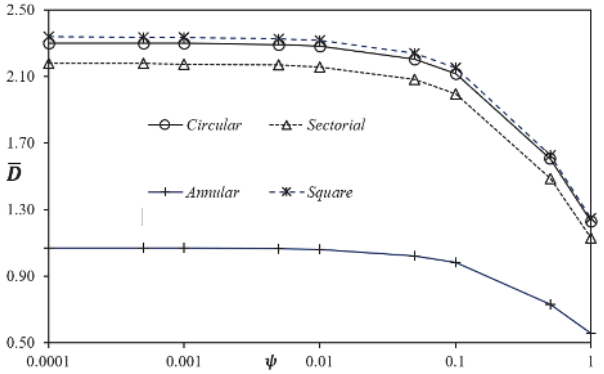

Fig. 8 Damping parameter vs permeability parameter

Table 2 Influence of film thickness on bearing performance indices

$\psi = 0.01$	$\bar{h}$	$\bar{F}_0$	$\bar{Q}$	$\bar{K}$	$\bar{D}$
Circular recess	0.2	1.6925	0.0272	0.0666	33.3485
	0.4	1.6200	0.1068	0.9217	10.3530
	0.6	1.2601	0.2538	2.4688	6.3109
	0.8	0.7871	0.3662	2.0190	3.8646
	1	0.4720	0.4248	1.1738	2.2820
Sectorial recess	0.2	2.1706	0.0541	0.3551	19.8676
	0.4	1.8698	0.1915	3.1187	11.1985
	0.6	1.1185	0.3497	3.5079	7.2867
	0.8	0.5914	0.4272	1.8329	3.8856
	1	0.3297	0.4609	0.8984	2.1593
Annular recess	0.2	2.2206	0.1111	0.3523	12.8676
	0.4	1.9210	0.1915	3.1975	5.3130
	0.6	1.1489	0.3499	3.6052	3.5614
	0.8	0.6074	0.4273	1.8823	1.9084
	1	0.3386	0.4609	0.9224	1.0621
Square recess	0.2	1.7420	0.0293	0.0779	31.5292
	0.4	1.6568	0.1146	1.0743	10.2927
	0.6	1.2567	0.2652	2.6379	6.5314
	0.8	0.7681	0.3744	2.0277	3.9556
	1	0.4558	0.4299	1.1494	2.3188

- The advantages offered by porous facing/layer such as self-lubricating and economical in use can only be beneficial if the value of permeability is less than 2.2×10^{-14} m^2 ($\psi < 0.01$), under given operating condition.
- The use of porous facing tends to marginally enhance the fluid flow requirement and pumping losses in bearing.
- A judicious selection of pocket shape can effectively counter partial loss in performance indices of bearing system occurred due to the use of porous facing. In this context, circular and square pockets should be preferred, as they offer better stiffness and damping capabilities to the bearing even at high porosity ($\psi > 0.01$).

References

[1] Rowe, W. B., "Hydrostatic and Hybrid Bearing Design," Butterworths, London, 2013.

[2] Osman, T. A., Dorid, M., Safar, Z. S. and Mokhtar, M. O., "Experimental Assessment of Hydrostatic Thrust Bearing Performance," Tribology International, 29, 3, 1996, 233-242.

[3] Wu, Z. and Dareing, D. W., "Non-Newtonian Effects of Powder-Lubricant Slurries in Hydrostatic and Squeeze-Film Bearings," Tribology Transactions, 37, 4, 1994, 836-842.

[4] Gohara, M., Somaya, K. and Miyatake, M., "Yoshimoto S. Static Characteristics of a Water-Lubricated Hydrostatic Thrust Bearing Using a Membrane Restrictor," Tribology International, 75, 2014, 111-116.

[5] Kumar, V. and Sharma, S. C., "Dynamic Characteristics of Compensated Hydrostatic Thrust Pad Bearing Subjected to External Transverse Magnetic Field," Acta Mechanica, 229, 2018, 1251-1274.

[6] Yang, H., Ratchev, S., Turitto, M. and Segal, J., "Rapid Manufacturing of Non-Assembly Complex Micro-Devices by Microstereolithography," Tsinghua Science & Technology, 14, 2009, 164-167.

[7] Coblas, D. G., Fatu, A., Maoui, A. and Hajjam, M., "Manufacturing Textured Surfaces: State of Art and Recent Developments," Proceedings of the Institution of Mechanical Engineers, Part J: Journal of Engineering Tribology, 229, 2015, 3-29.

[8] Costa, H. and Hutchings, I. M., "Some Innovative Surface Texturing Techniques for Tribological Purposes," Proceedings of the Institution of Mechanical Engineers, Part J: Journal of Engineering Tribology, 229, 2015, 429-448.

[9] Kumar, V., Sharma, S. C. and Narwat, K., "Influence of Micro-Groove Attributes on Frictional Power Loss and Load-Carrying Capacity of Hybrid Thrust Bearing," Industrial Lubrication and Tribology, 72, 5, 2019, 589-598.

[10] Gropper, D., Wang, L. and Harvey, T. J., "Hydrodynamic Lubrication of Textured Surfaces: A Review of Modeling Techniques and Key Findings," Tribology International, 94, 2016, 509-529.

[11] Kumar, V. and Sharma, S. C., "Study of Annular Recess Hydrostatic Tilted Thrust Pad Bearing under the Influence of Couple Stress Lubricant Behaviour," International Journal of Surface Science and Engineering, 11, 2017, 344-369.

[12] Kumar, V. and Sharma, S. C., "Combined Influence of Couple Stress Lubricant, Recess Geometry and Method of Compensation on the Performance of Hydrostatic Circular Thrust Pad Bearing," Proceedings of the Institution of Mechanical Engineers, Part J: Journal of Engineering Tribology, 231, 2017, 716-733.

[13] Boubendir, S., Larbi, S. and Bennacer, R., "Numerical Study of the Thermo-Hydrodynamic Lubrication Phenomena in Porous Journal Bearings," Tribology International, 44, 2011, 1-8.

[14] Murti, P. R. K., "Analysis of Porous Slider Bearings," Wear, 28, 1973, 131-134.

[15] Lin, J. R., "Optimal Design of One-Dimensional Porous Slider Bearings Using the Brinkman Model," Tribology International, 34, 2011, 57-64.

[16] Elsharkawy, A. A. and Guedouar, L. H., "Hydrodynamic Lubrication of Porous Journal Bearings Using a Modified Brinkman-Extended Darcy Model," Tribology International, 34, 2001, 767-777.

[17] Naduvinamani, N. B. and Siddangouda, A., "Effect of Surface Roughness on the Hydrodynamic Lubrication of Porous Step-Slider Bearings with Couple Stress Fluids," Tribology International, 40, 2007, 780-793.

[18] Naduvinamani, N. B., Fathima, S. T. and Jamal, S., "Effect of Roughness on Hydromagnetic Squeeze Films between Porous Rectangular Plates," Tribology International, 43, 11, 2010, 2145-2151.

[19] Madalli, V. S., Siddharama, P., Ayyappa, H. and Ramesh, K., "Analysis of the Viscosity Dependent Parameters of Couple Stress Fluid in Porous Parallel Plates," Industrial Lubrication Tribology, 70, 6, 2018, 1086-1093.

[20] Naduvinamani, N. B. and Hosmani, S. S., "Porous Exponential Slider Bearings Lubricated with MHD-Couple Stress Fluid," Industrial Lubrication and Tribology, 70, 5, 2018, 838-845.

[21] Hanawa, N., Kuniyoshi, M., Miyatake, M. and Yoshimoto, S., "Static Characteristics of a Water-Lubricated Hydrostatic Thrust Bearing with a Porous Land Region and a Capillary Restrictor," Precision Engineering, 50, 2017, 293-307.

[22] Dowson, D., "A Generalized Reynolds Equation for Fluid-Film Lubrication," International Journal of Mechanical Sciences, 4, 2, 1962, 159-170.

Nomenclature

A_b	Area of recess; (πR_o^2), mm^2
A_p	Area of recess; (πR_i^2), mm^2; $\left(\frac{A_b}{A_p} = 4\right)$
D	Damping coefficient of fluid film, N.s/m; $\left(\overline{D} = \frac{Dh_o^3}{r_o^4 \mu}\right)$
F_o	Fluid film reaction, N; $\overline{F}_o = \left(\frac{F_o}{p_s r_o^2}\right)$
h	Film thickness at any arbitrary point, mm; $(\overline{h} = h/h_o)$
$\dot{h}$	Runner squeeze/normal velocity, m/s; $\left(\overline{\dot{h}} = \frac{\partial \overline{h}}{\partial \overline{t}}\right)$
h_r	Nominal film thickness, mm
K	Stiffness parameter, N/mm; $\left(\overline{K} = \frac{h_o}{p_s r_o^2} K\right)$
p	Lubricant pressure, MPa; $\left(\overline{p} = \frac{p}{p_s}\right)$
p_{oc}	Fluid pressure in recess under steady state, MPa
R_i	Recess radius, mm
R_o	Thrust pad radius, mm
x, y, z	Cartesian coordinates, mm; $\left(\overline{x} = \frac{x}{r_r}; \overline{y} = \frac{z}{r_r}; \overline{z} = \frac{y}{h_r}\right)$
k	Permeability of porous facing m^2